Research article

Biosynthesis of iron oxide nanoparticles for the degradation of methylene blue dye, sulfisoxazole antibiotic and removal of bacteria from real water

Louisah M. Mahlaule-Glory [a], Sabetha Mapetla [a], Aubrey Makofane [a], Morongwa M. Mathipa [b], Nomso C. Hintsho-Mbita [a,*]

[a] DSI/NRF-CoE In Strong Materials, Department of Chemistry, Faculty of Science and Agriculture, University of Limpopo, Sovenga, Polokwane, 0727, South Africa
[b] Limpopo Agro-Food Technology Station, University of Limpopo, Sovenga, Polokwane, 0727, South Africa

HIGHLIGHTS

- Biosynthesis of Fe_3O_4 NPs using *M. burkeana* for the first time.
- 99% and 60% degradation of MB dye and antibiotic SSX, respectively.
- Superoxides were the major species responsible for MB degradation.
- Materials could be reused several times.
- High potency against gram positive strains using real water.

GRAPHICAL ABSTRACT
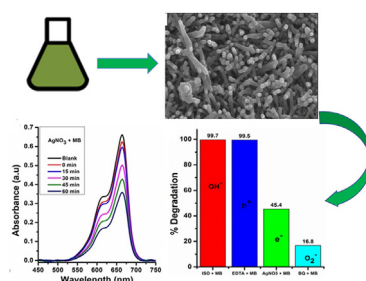
ARTICLE INFO

ABSTRACT

Water pollution that is caused by dyes, bacteria and antibiotics, has resulted in a threat to living organisms, animals and humans, hence there is a need to synthesize multifunctional materials that can be used for the degradation of various pollutants. The aim of this study was to synthesize Iron oxide (Fe_3O_4) NPs and test this material for photocatalytic degradation and antibacterial activity. The synthesis of Iron oxide (Fe_3O_4) NPs was conducted using *M. burkeana* extract and characterised using UV-vis, XRD, BET, SEM, EDS and TGA. The material was then tested for its photocatalytic and antibacterial efficiency against methylene blue dye, antibiotic sulfisoxazole and *E. coli* and *S. aureus* bacterial strains. XRD confirmed the formation of Fe_3O_4 NPs. UV-vis gave optical information whereby an excitation at 320 nm and a bandgap of 3.74 eV was noted. The deposition of the phytochemicals onto the Fe_3O_4 NPs was demonstrated using FTIR. From the surface analysis, the morphology of the synthesized NPs was found to be rod like and mesoporous. Upon testing for methylene blue degradation, the Fe_3O_4 NPs were more potent under basic conditions (pH 12) and the O_2 radicals were found to be the species responsible for the degradation. Against sulfisoxazole, a 60% degradation was observed. Lastly, when testing these materials against bacterial strains found in tap, pond, river and sewage water, they were potent in particular against gram positive strains. These results show that at optimum conditions, these materials are able to degrade various pollutants in wastewater.

---

* Corresponding author.
  E-mail address: nomso.hintsho-mbita@ul.ac.za (N.C. Hintsho-Mbita).

1. Introduction

The increase in human population worldwide, has necessitated the need and expansion of industries such as the textile and pharmaceutical industry, where dyes are required to change the colour of the cloths and the antibiotics are for human treatment [1]. Consequently, the demand has increased thus leading to a large production and large quantity usage. The improper disposal and direct discharge of dyes and pharmaceutical pollutants generated from the textile industries and the hospital effluents has led to water pollution within the ecosystem [2]. Toxins from these effluents enter the water bodies and worsen the quality and condition of the eco-system globally, thus making drinking water unstable for consumption [3, 4]. Water is the source of life and exposure to these toxins badly affects the ecosystem placing animals and human health at risk [5]. Organic dyes are notorious for causing damage to the central nervous system, gastrointestinal and respiratory diseases [6]. Also, the increased usage of antibiotics may cause irreversible and long term effects to microbes by leading to genetic exchange, consequently accelerating the resistance of (bacteria species) pathogens against antibiotics [6]. Thus promoting human health threat when disorders, syndromes and disease are therefore developed [7, 8].

Several methods such as floatation, ion exchange, chlorination, adsorption, electrochemical and photocatalytic degradation have been used for the removal of dyes, bacteria and pharmaceutical drugs in water in particular pollutants such as methylene blue (MB), malachite green (MG), *E. coli,* Amoxicillin, Diclofenac, *S. aureus*, ciproflaxin, sulfamethoxazole (SMX) and sulfisoxazole (SSX) respectively [4, 6]. A majority of these methods are expensive, require sensitive equipment and the products cannot be reused [7, 8]. For ion exchange, the pre-treatment of all the samples is always a requirement and for biological methods, standardization is required and in most cases, these methods have a poor efficiency. Of these methods, photocatalysis is the most preferred method by researchers as it has been shown to degrade complex pollutants, is easy to use and can produce reproducible results [9, 10, 11].

Metal oxides such as Zinc Oxide (ZnO), Iron Oxide (Fe$_2$O$_3$), Titanium dioxide (TiO$_2$), Nickel Oxide (NiO) *etc* have been used as photocatalysts for the degradation of various pollutants from wastewater [12, 13, 14]. Of these, TiO$_2$ and ZnO are the most commonly used semiconductors due to their photoelectric properties, thus extensive studies have focused on these materials. Akinola *et al* synthesized multifunctional TiO$_2$ using the extracts of *Cola nidita* [3]. At optimum conditions, a maximum degradation of 86% was achieved for malachite green dye. Ngoepe *et al* also synthesized green TiO$_2$ using *Monsonia Burkeana*, a 85% degradation of MB was achieved [15]. From these studies, it can be noted that the traditional green derived semiconductors are also highly effective even though they still suffer from known limitations such fast recombination rate, broad bandgap, reusability etc. Moreover, because they are green derived, they are less toxic and due to that these materials can also be used in a variety of other applications in particular the biomedical field as anticancer, antioxidant and antibacterial agents. Of interest lately has been Iron oxide nanoparticles. These materials are preferred since they generally have a low bandgap but more importantly because they are magnetic, which means that they can also be easily recovered during the water treatment process.

Of interest lately has been Iron oxide nanoparticles. These materials are preferred since they generally have a low bandgap but more importantly because they are magnetic thus making them recyclable. These materials can be classified in to three categories, namely, Hematite (α Fe$_2$O$_3$), Maghemite (γ Fe$_2$O$_3$) and the magnetite (Fe$_3$O$_4$) [2,9]. Hematite is the most preferred form as a photocatalyst, where-as maghemite and magnetite are primarily used for drug delivery, energy storage and data storage [10]. The degradation of pollutants using iron-based materials depends on the stability and the surface area of the material. Thus, this necessitates a synthetic method that can achieve that. Synthesis strategies such as sol gel, chemical vapour deposition and pyrolysis have been found to promote the usage of unsafe, hazardous solvents and with synthesis conditions requiring extremely high pressures and temperatures. Furthermore, they generate a large surface ratio and higher energy levels on the surface of the material [11, 12]. Moreover, the chemical synthesis methods tend to affect the iron-based nanoparticles by reducing their magnetic properties. This is because, in chemical synthesis, the iron-based nanomaterials are easily oxidized by high chemical activity resulting in loss of the magnetic property of the material [13]. Thus, researchers have moved towards the use of safer materials through green chemistry.

Green chemistry is an area in science, which aims at synthesizing materials that are environmentally friendly through the use of plant extracts, fungus and bacteria to name a few [14, 16]. The use of plants extracts for the synthesis is more preferred as this method has the ability to reduce the energy levels, increase neutrality and also display the ability to oxidize [17]. Moreover, green synthesis is not time-consuming, does not require several steps and the plants are mostly readily available. The plant extracts have been shown to consists of phytochemicals such as *terpenoids, tannis, polyphenols* which are rich in hydroxyl and carboxylic groups which normally act as reducing agents for the synthesis of nanoparticles [15, 18, 19]. Several studies have shown that biomedical synthesis of iron oxide nanoparticles have been effectively used in the degradation of pollutants. Bibi *et al* [6], synthesized iron oxide using the *promegrenade* seeds for the removal of reactive blue dye. The study showed a degradation of 95% of the dyes using a spherical nanomaterial with the sizes of 25 and 55 nm. Another study was performed for the removal of Remazol yellow (77%) dye by the green (*Carica papaya* leaf extract) derived iron oxide nanoparticles [7]. *Canthium coromandelicum* leaf extract was used to synthesize iron oxide nanomaterial and used for the degradation of Janus green dye, a 97% degradation was obtained [20]. From these studies, it could be noted that iron oxide nanoparticles were highly efficient in the degradation of dyes.

In this study, a low cost, green and recyclable material, Iron oxide (Fe$_3$O$_4$) nanoparticles was synthesized using *M. Burkeana* plant extract for the degradation of methylene blue dyes and sulfisoxazole antibiotics in wastewater. The effect of pH against the MB dye, surface analysis, spectroscopic, thermal stability studies, reactive oxygen species and reusability studies were conducted. Furthermore, the activity of this material against the sulfisoxazole antibiotic was also evaluated. Lastly, the potency of this material against Total Coliforms, *E. coli* and *S. aureus* against real water pollutants was also investigated.

2. Materials and methods

2.1. Materials

All the chemicals used for the preparation of the photocatalysts and photodegradation experiment studies were of analytical grade. Methylene blue dye (MB) (C$_{16}$H$_{18}$ClN$_3$S, Sigma-Aldrich), Iron nitrate nonahydrate Fe(NO$_3$)$_2$.9H$_2$O, 98%; Sulfisoxazole (C$_{15}$H$_{24}$N$_4$O$_5$S, >98%) were purchased from Sigma Aldrich and used in their original state.

A membrane filter with a pore size 0,45 μm and 47 mm diameter were purchased from Sigma Aldrich, Germany. *M. burkeana* plant was harvested from the Limpopo Experimental Farm, Mankweng.

2.2. Extraction of M. burkeana plant

The method used for the extraction of *M. Burkeana (MB)* was reported by Motene *et al.* [18]. Briefly, 5 g of *M. burkeana* plant powder was added to 250 ml of hot water and allowed to boil at 80 °C for 15 min. The extract was cooled down at room temperature and was filtered using the 0.45 filters through gravity filtration. Upon collection, the extract was stored in the refrigerator at 4 °C until further use.

2.3. Synthesis of Fe$_3$O$_4$ using M. burkeana plant extract

The synthesis Fe$_3$O$_4$ NPs was conducted using a wet chemistry technique. Briefly, 0.1 L of the prepared *M. Burkeana* extract was poured in to

a 1 L beaker. Thereafter, 0.4 L of a 0.1 M ferric hexa-hydrate solution was poured in a dropwise motion at a slow pace to the *M. burkeana* plant extract solution, to allow the reaction to take place accordingly. As the reaction was taking place, a change of colour and formation of pre-cipitates indicated the formation of nanoparticles. After the formation of the bubbles had stopped, the reaction was presumed to be complete. The Fe_3O_4 nanoparticles were filtered using the filtration system with the 0,45 μm membrane filters. The residue was also washed with methanol and distilled water. The resulting nanoparticles were dried at 50 °C.

2.4. Characterization

To study the morphology and particle size distribution of Fe_3O_4 NPs, a Zeiss Auriga Scanning Electron Microscopy (SEM) instrument was used. Crysallite sizes, phase identification and crystallinity were studies through the use of X-Ray Diffraction (XRD) using a Philips PW 1830 at a scan range of 0–80°. To confirm the formed nanoparticles, FTIR (Bruker, Alpha) using a scan range of 500–4500 cm^{-1} was conducted. Furthermore, the phyto-chemical analysis from the plant deposition was also determined. To un-derstand their thermal stability, a Pyris PerkinElmer system was used, where the Fe_3O_4 samples were heated to 900 °C at a flow rate of 10 °C/min under air gas. Lastly, the surface area analysis and pore size measurements were conducted using a BET Micrometrics Tri Star.

2.5. Photocatalytic degradation of MB dye using iron oxide nanoparticles

The photocatalytic degradation of Methylene blue (MB) dye using Fe_3O_4 nanoparticles was studied using a 150 W UV lamp following a method reported previously by several authors [15, 18]. Briefly, the ef-fect of pH was investigated whereby pH 3, pH 7 and pH 12 were the conditions of choice. In these degradation experiments, in a 250 ml beaker, 25 mg of the Iron oxide photocatalyst was added to 100 ml of the 5 ppm MB solution. Prior to the light being emitted on the solution, an adsoption-desoption experiment was conducted in the darkness for about 30 min to achieve equilibrium. Thereafter, the solution was exposed to the UV light for 60 min. At 15 min intervals, 5 ml of the solutions were aliquoted and taken for analysis using a UV-Vis spectrophotometer at a wavelength of 668 nm. The percentage degradation was calculated as follows, using Eq. (1):

$$\% \ \text{Degradation} = \frac{(A_0 - A_t)}{A_0} \times 100 \tag{1}$$

where "A_0" indicates the initial absorption of the MB dye solution and "A_t" indicates the final absorption of the MB dye at specified time intervals.

2.6. Reusability and stability studies

The reusability and recovery of the Fe_3O_4 NPs towards the degrada-tion of MB dye was studied using a method reported previously. More than four trials were conducted and after each trial, the photocatalyst was removed from the solution through centrifugation, washed several times thoroughly with deionized water, and then dried in an oven for 60 min at 80 °C.

2.7. Influence of reactive species on the photocatalytic degradation of MB dye

The effect of reactive species on the degradation of MB dye was investigated through the addition of B-benzoquinone, EDTA, isopropyl alcohol and $AgNO_3$ as the main scavengers for O_2, h^+, •OH, and e^- radicals, respectively, in the experiments. Upon testing the effect of these species, the experiments were conducted the same way as the normal degradation experiments except that 2.0 mmol/L of the different scav-enger solutions were added.
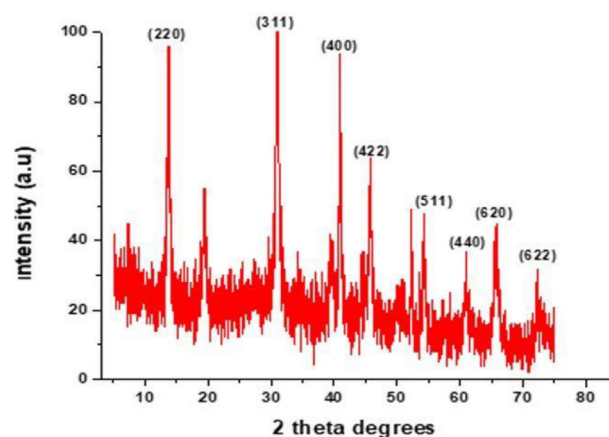

Figure 1. XRD analysis *M. burkeana* synthesized Fe_3O_4 NPs.

2.8. Photodegradation of the antibiotic sulfisoxazole

The photocatalytic degradation of antibiotic sulfisoxazole (SSX) was conducted using a 150 W UV lamp. Briefly, 100 mg of Fe_3O_4 NPs was added into a 100 mL 10 ppm SSX solution. To ensure an adsorption-desorption equilibrium, the solution was stirred for 30 min in the dark prior to irradiation. Thereafter, the mixture was exposed to UV-light irra-diation for 2 h. At 30 min intervals, about 3 ml aliquots of antibiotic so-lution were drawn of the solution and the rate of decomposition was determined using a UV-vis spectrophotometer at 285 nm in the process.

2.9. Antibacterial activity of Fe_3O_4 NPs against various bacterial pollutants

The antibacterial activity of *M. burkeana* Fe_3O_4 NPs against the *Total Coliform*, *E. coli* and *S. Aureus* was investigated following the method described previously [18] without any modification. From the analysis, 4 water samples from the river, tap, pond and sewage were investigated. In this study, 2 concentrations (5 and 50 mg/L) of the catalyst were added onto the various water samples, allowed to be incubated for overnight at 37 °C and after the treatment, analysis was taken using the tempo reader.

3. Results and discussion

3.1. Phase identification and structural analysis (XRD)

X-ray diffraction analysis was conducted for the plant synthesised Fe_3O_4 NPs in order to gain knowledge regarding the structural features of the synthesized nanoparticle. In Figure 1, the characteristic diffraction peaks for Fe_3O_4 were observed and assigned as follows (220), (311), (400), (422), (511), (440), (620) and (622) corresponding to the following 2θ values 14, 30, 35, 41, 45, 54 and 62, 66, 74° respectively [21, 22]. The diffraction pattern for the plant synthesised Fe_3O_4 NPs (JCP 22_33-0664) matches those of previously published chemical synthesized materials except the green materials have additional peaks and a slight peak shifting may have occurred, whereby they were also a bit broader, which then would also have an effect on the particle size of these ma-terials [23]. These results corroborate with work that was done by Yogamoorthi *et al.* [24] and Latha *et al* [17] from the XRD pattern ob-tained when Fe_3O_4 NPs were synthesized using papaya leaves.

Generally, the mechanical and physical properties of nanomaterials mostly depend on how crystalline the material is and their size. When a material is highly crystalline and has a small crystalline size, it is mostly expected that these properties could enhance their photocatalytic ca-pacity. From the Debye-Scherer equation, the green synthesized nano-particles were calculated to be 60.2 nm. To obtain more information about the materials, Optical analysis was conducted to obtain more in-formation about the functional groups and the formation of the material.
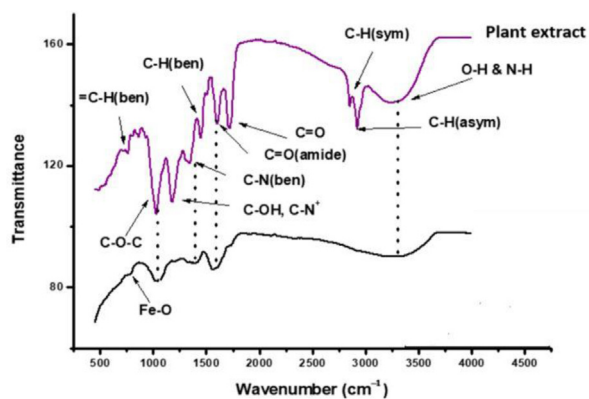
Figure 2. FTIR analysis of *M. Burkeana* plant extract and Fe_3O_4 NPs.

3.2. Optical analysis via UV-vis and FTIR

Fourier Transform Infrared Spectroscopy (FTIR) was used to identify the functional groups found in the plant and the formed nanoparticles. The *M. Burkenana* plant extract and Fe_3O_4 nanoparticles both showed a stretch at 3250 cm^{-1}, which was assigned to O–H and N–H, indicating the presence of phenolic compounds. These are the functional groups of the biomolecules which are responsible for the reduction, capping and efficient stabilization of the metal ion precursor to its corresponding nanoparticles. Other groups from the plant extract that have been integrated onto the Fe_3O_4 NPs as shown by dotted lines in Figure 2 are C–O–C, C–N$_{(bent)}$ and C=O$_{(amide)}$ at 1100, 1300 and 1600 cm^{-1}, respectively. The peak in the fingerprint region at 750 cm^{-1} due to Fe–O confirmed the formation of Fe_3O_4 NPs [15, 23]. Senhil *et al* (2022) synthesized Fe_3O_4 NPs at room temperature using *Tridax procumbens* plant extract and reported that the carbohydrates from the plant extract acted as the reducing agents [20]. Hydrogen bonded (OH) groups were also identified at 3446 cm^{-1} and 1611 cm^{-1}. The presence of carboxylic groups (–COOH–) at 1300 cm^{-1} were also identified, these are known to be responsible for the formation of Fe_3O_4 nanoparticles and C–O–C stretching frequency.

How iron oxide nanoparticles normally form from the use of plants as a reducing agent is not well understood but several authors have

suggested that the formation could be a two-step reaction mechanism. In this process, the phytochemicals identified which contain the hydroxyl and aldehyde groups generally play a role in the partial reduction of Fe^{3+} to Fe_3O_4 nanoparticles. The hydrolysis of $FeCl_3$ to $Fe(OH)_3$ takes place and it is followed by the release of H^+. Juarez-Rojop et al 2014, further explained that phytochemicals such as tannis, flavonoids and phenols, which are some the phytochemicals found in the *M. burkeana* plant extract in this study act as both reducing and stabilizing agents during synthesis. Anchan *et al.* 2019, stated that the formation of the brown colour, the bubbles and precipitation as noted in this study, were caused by the reaction between the phytochemicals and the metal ions and served as an indication that the iron oxide NPs had formed. Devi et al., 2019 also elaborated that though many reactions take place when the iron salt is reacted with the extracts, it does not reduce Fe^{3+} to Fe^0 as oxidation takes place, instead the phytochemicals react with the ions of the iron to form the NPs [9]. To further understand the potential characteristics of these materials, UV-vis DRS was conducted as it is known that optical properties of semiconducting materials are strongly linked to their optical absorption capability which might later affect their photocatalytic activity.

In Figure 3a, the UV-vis showed that the material got excited at 320 nm, which confirmed the formation of Fe_3O_4 as this was a characteristic feature of Iron oxide nanoparticles. This result was further corroborated by Lakshminaranayan *et al.* [13] and other researchers whereby they found that Iron oxide peaks are normally found between 300–350 nm. This also depending on the phytochemicals used as reducing agents for the synthesis of green derived Iron oxide nanoparticles. It is known that iron nanoparticles generally absorb a certain amount of UV radiation which is caused by the movement of the electrons from the valence band to the conduction band. The bandgap was also measured (Figure 3b) through the Tauc plot where it was found to be 3.75 eV. Morphological analysis of this material through SEM/EDS for the plant derived Fe_3O_4 was conducted to obtain more information.

3.3. Morphological analysis

SEM and EDS analysis was conducted to determine the morphology and elemental composition of the synthesized Fe_3O_4 NPs. Figure 4(a, b, c) shows the morphology of the Fe_3O_4 NPs to be rodlike. This was different from what was observed by Pattanayak *et al.* (2013) who successfully

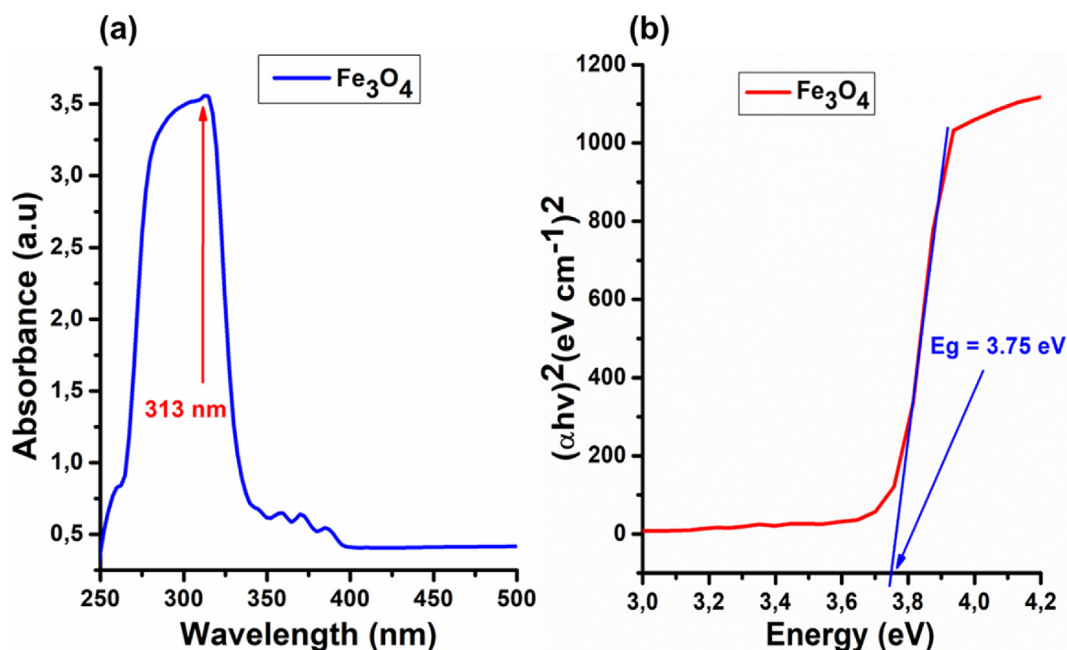**Figure 3.** (a) UV-vis plot of Fe_3O_4 and (b) Taucs plot of Fe_3O_4.

(e) Element	Wt%	Wt% Sigma
C	6.52	0.08
O	28.57	0.12
Fe	64.91	0.23

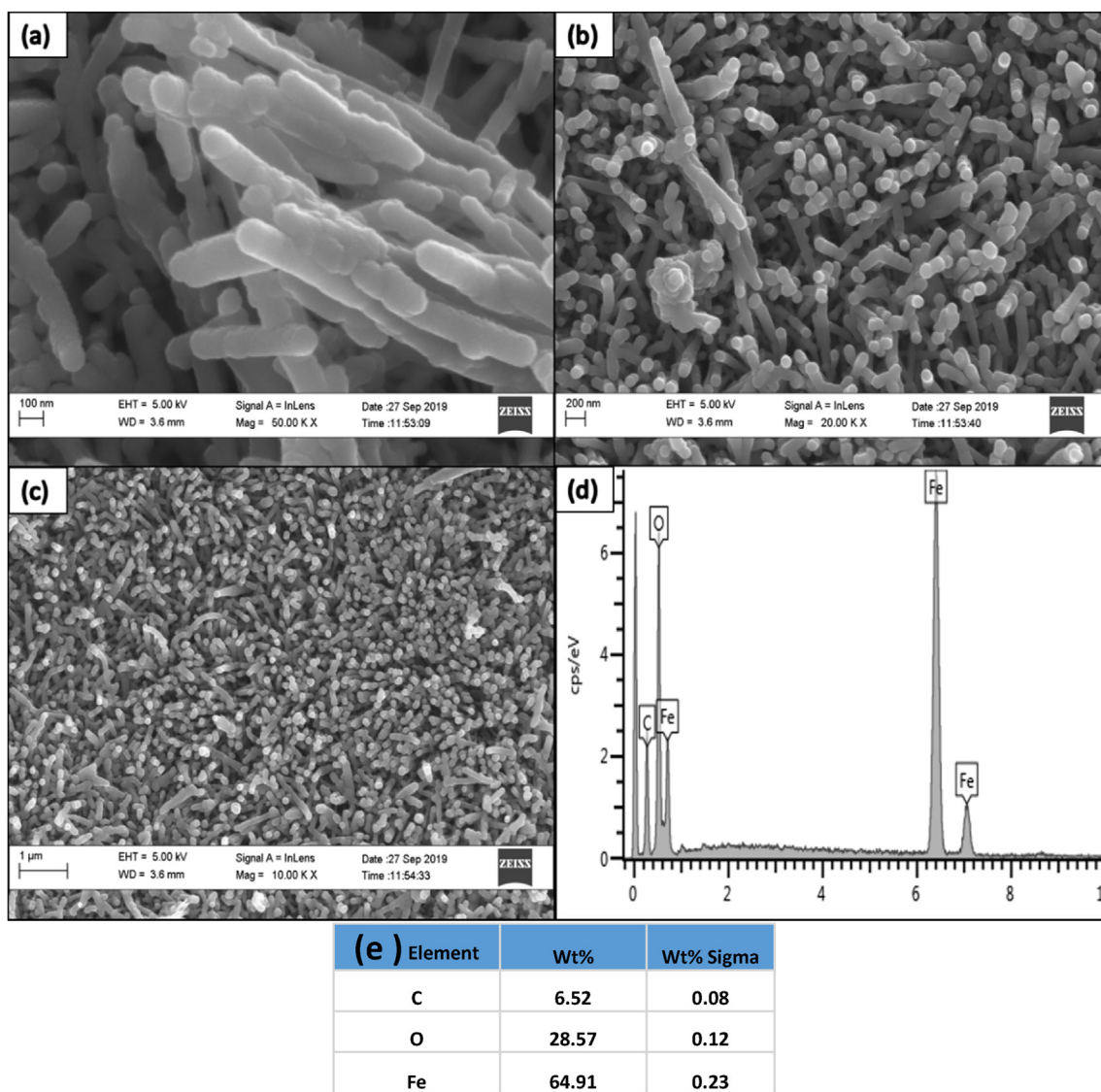**Figure 4.** (a, b, c) SEM at various magnifications, (d) EDS of Fe_3O_4 NPs and (e) Weight.

synthesized Fe_3O_4 NPs using various plant extracts. The SEM image of the synthesized NPs revealed they were mostly spherical in shape [25]. These differences could be due to the varying phytochemicals identified in the plant which could have played a role in the formation of spherical and rodlike Fe_3O_4 nanoparticles. Figure 4(d) shows the elemental composition of the Fe_3O_4 NPs which demonstrated that the elements Fe and O are in abundance (Figure 4e), confirming the formation of the NPs in addition to the C peak, identified to be from the plant extract [21]. To understand the thermal stability of the synthesized Fe_3O_4 NPs, as it is an important factor in catalytic activities, TGA was conducted.

3.4. Thermal stability of Fe_3O_4 NPs

The percentage weight loss was studied by TGA for green synthesized Fe_3O_4 NPs. The purpose of this was to investigate the decomposition and to gain structural information about the NPS. From Figure 5(a), the TGA curve shows a weight loss over the range. Four derivative peaks in the DTG curve (Figure 5b), (more than three for Fe_3O_4 NPS implying the presence of impurities) were identified which correlated to the mass losses found in the TGA curve. The peak just under 100 °C, had a mass loss of 22%, was due to decomposition of water, caused by the OH groups present in the Fe_3O_4 NPs. A peak at 280 °C, with a percentage mass loss of

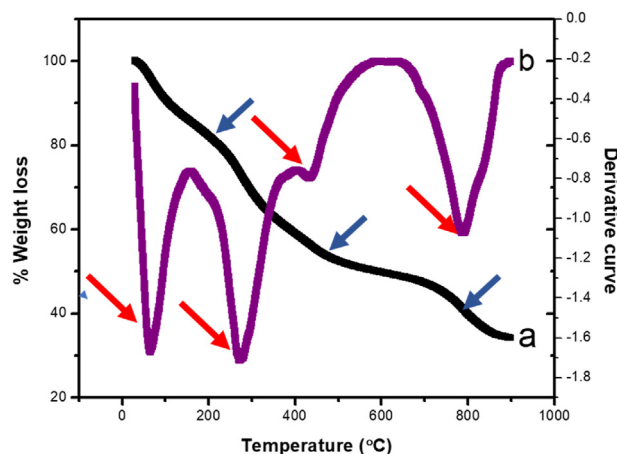**Figure 5.** (a) TGA and (b) DTG of Fe_3O_4 NPs.

5% was caused by the decomposition of the protein chains from the plant extract. At 444 °C, a percentage weight loss of 15% due to the capping agents from the plant extract in the Fe_3O_4 NPs was noted. The last peak at
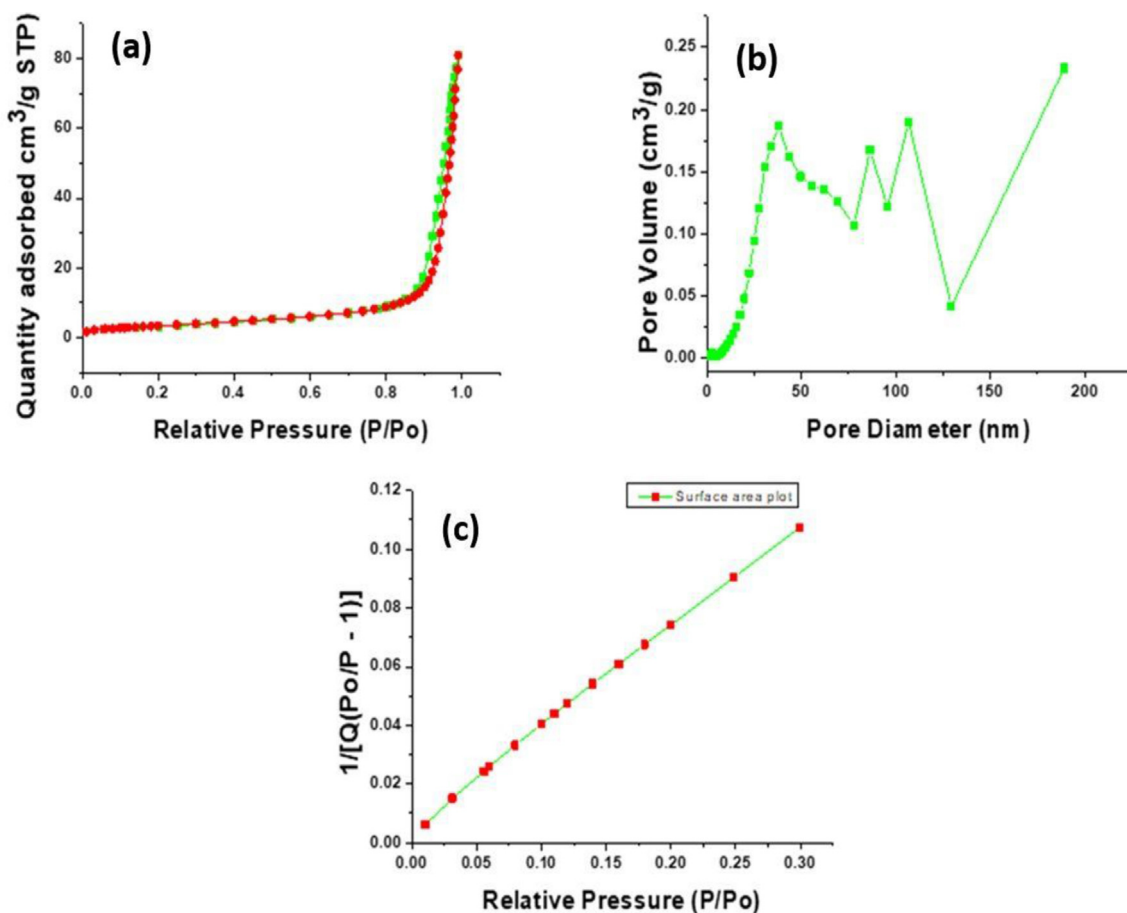
Figure 6. (a, b, c): (a) The adsorption-desorption isotherm, (b) the pore size plot and (c) the surface area plot of Fe_3O_4 NPs.

Table 1. Comparison of green derived Iron Oxide nanoparticles for dye degradation.

Plant	dosage (mg)	Time (min)	Dye	pH	% Removal	Refs.
Carica papaya	800	250	RRRY	2	76	Bhuiyane *et al.* [6]
Withania coagulans	5	180	Saffarin	NR	68	Qasim *et al.* [26]
Ruellia tuberosa	-	150	CV	NR	79	Vasantharaj *et al.* [27]
Canthium coromandelium	10	180	Janus Green	NR	97%	Sudhakar *et al.* [9]
Chlorophytum comosum		360	MO	NR	77	Ardakani *et al.* [5]
Monsonia burkeana	**25**	**30**	**MB**	**12**	**99.8%**	**Present study**

*RRRY-Remazol RR Yellow *CV-Crystal Violet *NR-Not recorded.
*MB-Methylene Blue * JG-Janus Green.

780 °C, with a mass loss of 15% could have been due to phase transition from Fe_3O_4 to FeO since it has been shown that FeO is highly stable beyond 570 °C.

3.5. Surface area studies (BET)

BET analysis (Fig. 6a, b, c), was conducted in order to gain information regarding surface properties such as surface area, pore size and volume of the green synthesised Fe_3O_4 NPs. The results for this experiment are given in Table 1. The surface area was shown to be 12.83, with a pore size of 35.67 nm, which falls within the range 2–50 nm implying that the sorbent is mesoporous Venkateswarlu *et al.* (2013) synthesized green iron oxide NPs using *plantain* leaf extract. The surface area of the synthesized NPs was comparable to the one reported in our study and found to be 11.31 mg^2/g. The structure of the NPs was assigned to be mesoporous based on the BET surface area and pore volume results. This data clearly shows that Fe_3O_4 NPs can be used as a photocatalyst for the degradation of various pollutants from wastewater.

3.6. Effect of pH on the degradation of MB using Fe_3O_4 NPs

The pH is one of the most important factors to be considered when testing a material's ability to degrade. In this study, the effect of pH (Figure 7a, b, c, d) was investigated, whereby acidic, neutral and highly basic conditions were created. From the analysis, pH 12 (basic conditions), produced the highest degradation of 99% in less than 30 min. This is because MB dye as a thiazine dye has a cationic nature that tends to dissociate into negatively charged ions, especially at pH 12 [2]. This then increases the OH^- ions on the surface of the material. Thus increasing the OH^- radicals as active sites on the surface [23]. This leads to a higher and complete degradation percentage of MB. Moreover, since Iron oxide materials are magnetic, it therefore, would have undergone the electric
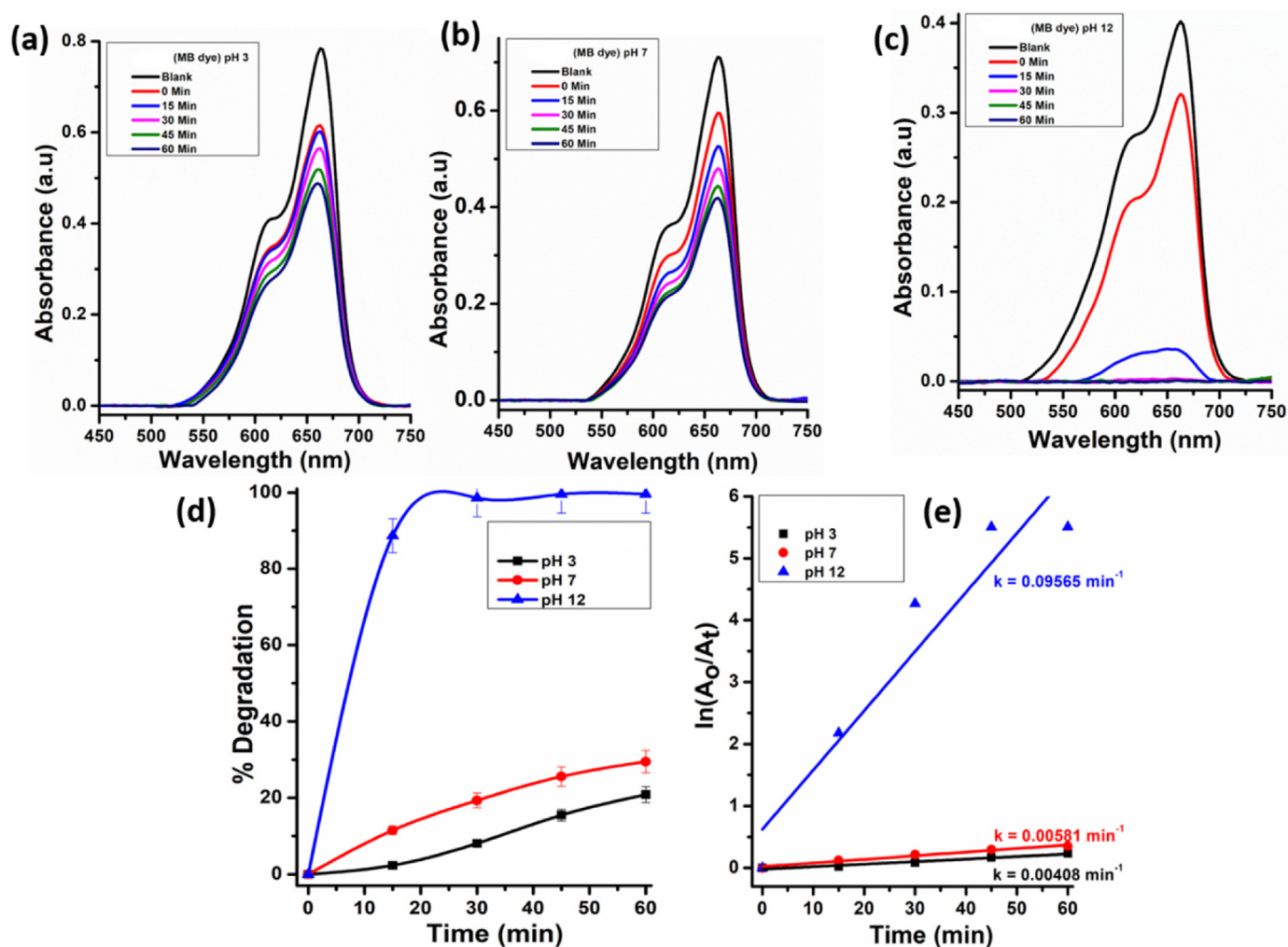
Figure 7. (a, b, c) the pH study during degradation, (d) degradation % and (e) the rate of reaction at different pH values.

dipole moments where the positively and negatively charged ions are easily separated, thus allowing the surface material to adsorb and degrade the dye [26, 25, 28]. These results showed an improved and complete degradation of MB dye within 60 min. Various studies also reported a degradation of more than 95% for MB at basic conditions [6, 26]. At pH 3, the lowest degradation of 18% was noted. This is because at acidic conditions more positively charged ions are formed and when they interact with a cationic dye they tend to form repulsion, thus exhibiting minimal dye degradation. At neutral conditions though, not much degradation was noted, with only 25% of MB degraded.

The rate of the reaction was also investigated as exhibited in Figure 7(e). The photocatalytic results were calculated using the Langmuir Hinshelwood equation:

$$\ln(C_o/C_t) = kt$$

Where the rate of the reaction is represented by the ln, C_o is the initial concentration, C_t is the final concentration, k is the rate of reaction constant and t is reaction time [19]. According to the plotted results indicated in Figure 7(e), the rate of the reaction is following the Pseudo first-order kinetic with the kinetics rate equal to k = 0.096 min^{-1}, thus leading to the fastest rate of reaction conducted at pH 12 than the rest of the pH measurements. When comparing our results with previously published data, it can be noted that iron oxide nanoparticles are effective in dye removal in general [29, 30]. Bhuiyan *et al.* got a 99% removal at basic conditions of pH 12 as well with the minimal rate of 0.008 min^{-1} following first order ($R^2 = 0.99$) kinetic. Another study, followed first order $R^2 = 0.9943$ kinetic with the rate of 0.00016 min^{-1}

[31] Also importantly to note, our green derived Fe_3O_4 was highly efficient for dye degradation as a 99% efficiency was noted for MB at 30 min, whereas for other studies (Table 1) a longer period of time (300 min, 250 min, 180 min *etc)* was required to have a high degradation. Moreover, in some instances a higher catalyst amount (800 mg) with prolonged periods was required but still not a complete degradation was achieved. It can also be noted also that in all the studies, different dye pollutants were used, as that maybe could also play a role in the differing degradation efficiencies. The complex aromatic nature of the various dyes is one of the reasons that has made researchers to move towards the synthesis of multifunctional materials, that can be used for the removal and degradation of various pollutants. The reusability studies were performed for 4 trials to assess the stability and the reusability property of our material.

3.7. Reusability studies of Fe_3O_4 NPS against MB dye

The reusability studies of Fe_3O_4 NPs was evaluated at optimal conditions of 25 mg dosage, 5 ppm concentration and pH 12 for 4 cycles (Figure 8a, b, c, d). The stability of a material is an important factor as it also contributes to the cost factor of the synthesized materials. The results illustrate that the material is stable and maintained its excellent photocatalytic efficiency. This is noticed when the degradation activity of all these cycles obtained was above the 98% degradation even with the last cycle (Figure 8e). Since the stability and the recyclability efficiency was perceived, the reactive species responsible for the degradation of MB and the mechanism is further explored in the following section.
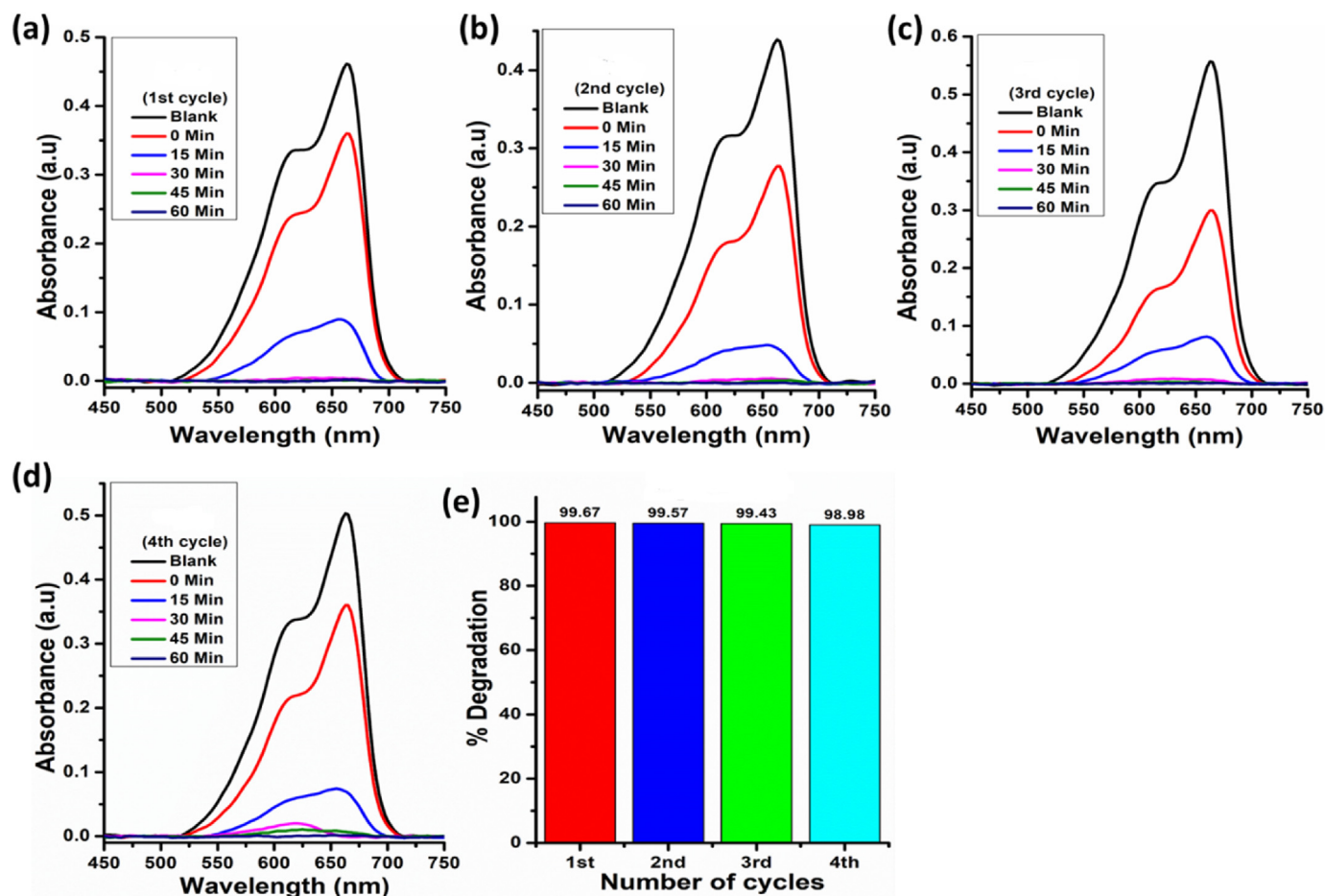
Figure 8. (a, b, c, d) Four experimental trials of Fe_3O_4 material against MB and (e) the degradation activity of these trials.

3.8. Effect of reactive species on the degradation of MB and mechanism

P-benzoquinone, EDTA, isopropyl alcohol and $AgNO_3$ were used as the four quenchers, to evaluate the contribution of scavengers and which one was responsible on the degradation against MB dye. The reactive species (main scavengers) of superoxide (O_2), holes (h^+), hydroxyl radicals (•OH), and electrons (e^-) radicals, respectively were added to the trapping experiments [15]. Upon testing the effect of these species, the experiments were conducted the same way as the normal degradation experiments except that 2.0 mmol/L of the different scavengers were added. The results from the trapping studies are displayed in Figure 9(a, b, c, d).

From the results (Figure 9e), it can be noted that the degradation of MB was not affected by the addition of OH and h + quenchers. However, trappers such as the electrons (e−) and O_2 radicals played a major role as the degradation of MB decreased to 45.4 and 16.8 respectively. The O_2 radicals were the major species responsible for the degradation. The study done by Makofane et al. [15], showed that electrons were the main contributors to the degradation process. This could have been because their material was a metal iron-based material for the removal of dye. Other authors also had the most effective species as a superoxide which correlates with our study, followed by the hydroxyl and the electrons. Whereas in our study, the most effective reactive species are the superoxide, followed by the electrons for the photocatalytic degradation. This shows that when there was enough light absorbed on the Iron oxide surface (Scheme 1) and they had reached the valence band (VB), the excited e^- moved to the conductive band (CB) whilst leaving the holes behind. In the process, the O_2 and OH radicals were also forming and as noted in radicals. The O_2 radicals which were absorbed on the surface of the material, contributed to the removal of MB dye during photocatalytic

degradation. Our material was further evaluated for the photodegradation of the SSX antibiotic pollutant.

3.9. Photodegradation of antibiotic sulfisoxazole (SSX) using Fe_3O_4 NPs

Suflonamides are pharmaceutical pollutants that have gained a lot of attention in the last decade due to the increased over reliance on medications such as antibiotics. Through excretion and urine feaces, these antibiotics have found their way into the water streams and the concentrations are increasing uncontrollably, hence the need for viable methods and newer materials to be used. In this study, the effect of time on the degradation of Sulfisoxazole (SSX) was investigated. The UV-Vis spectra of the results are exhibited in Figure 10(a). It can be noted that the degradation effect was monitored over 120 min at 30 min intervals. A maximum degradation of 60% was achieved after 120 min. These results also indicate that the degradation of SSX using Fe_3O_4 followed second-order kinetic as displayed in Figure 10(c). When comparing with the previously published work, a 67% degradation was noted against SSX using a nickel ferrite nanoparticle [15]. When iron oxide was degraded against another antibiotic, tetracycline, a low degradation of 40% was achieved [21]. They noted that when there is a high level of adsorption taking place between the catalyst surface and the pollutant before degradation occurs, photodegradation of the antibiotic might be impared. Lack of penetration of light might take place due to the screening, which would then mean that the formation of the excited electrons and holes might be limited. To further test potency of this material against other pollutants, the antibacterial efficiency of this material against various bacterial strains from real water samples was investigated.
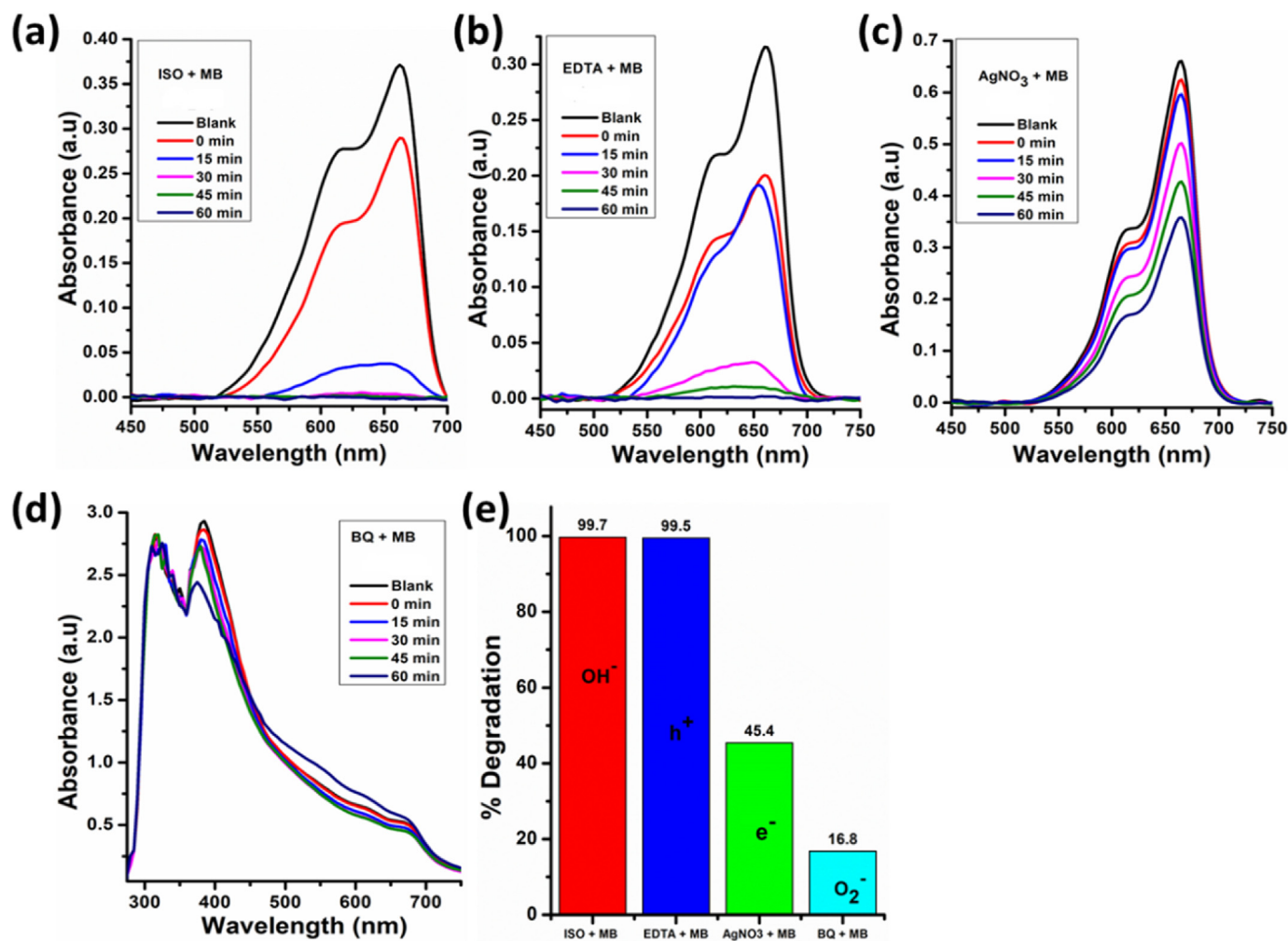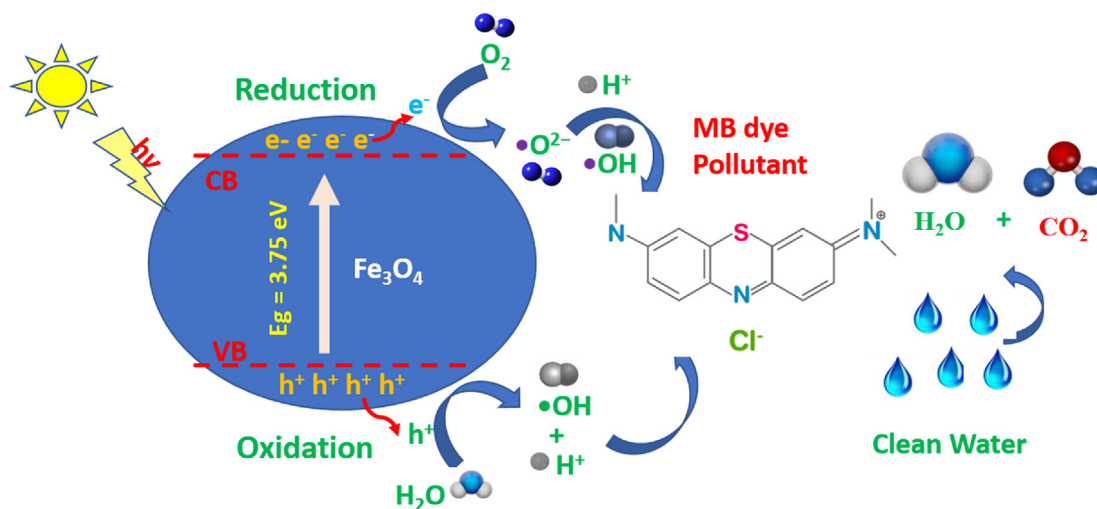
**Figure 9.** (a, b, c, d) the degradation of the scavengers and (e) the percentage degradation of active species.

Scheme 1. Schematic depicting photocatalytic degradation of MB dye.

3.10. Antibacterial efficiency of M. Burkeana Fe_3O_4 NPs against various strains

The antibacterial potency of *M. Burkeana* Fe_3O_4 NPs was investigated against Total Coliforms, *E. Coli* and *S. Aureus*. From Table 2, it can be noted that water from the pond, river, tap and sewage was investigated.

In all the water types, a high number of total coliforms in particular for sewage water was detected. This could be due to the fact that total coliforms generally consist of all the different types of bacteria as there is no classification or differentiation from the other strains. In pond, river and tap water there was no gram negative *E. coli* detected and in tap water even the gram positive *S. aureus* was not identified. Only in sewage water
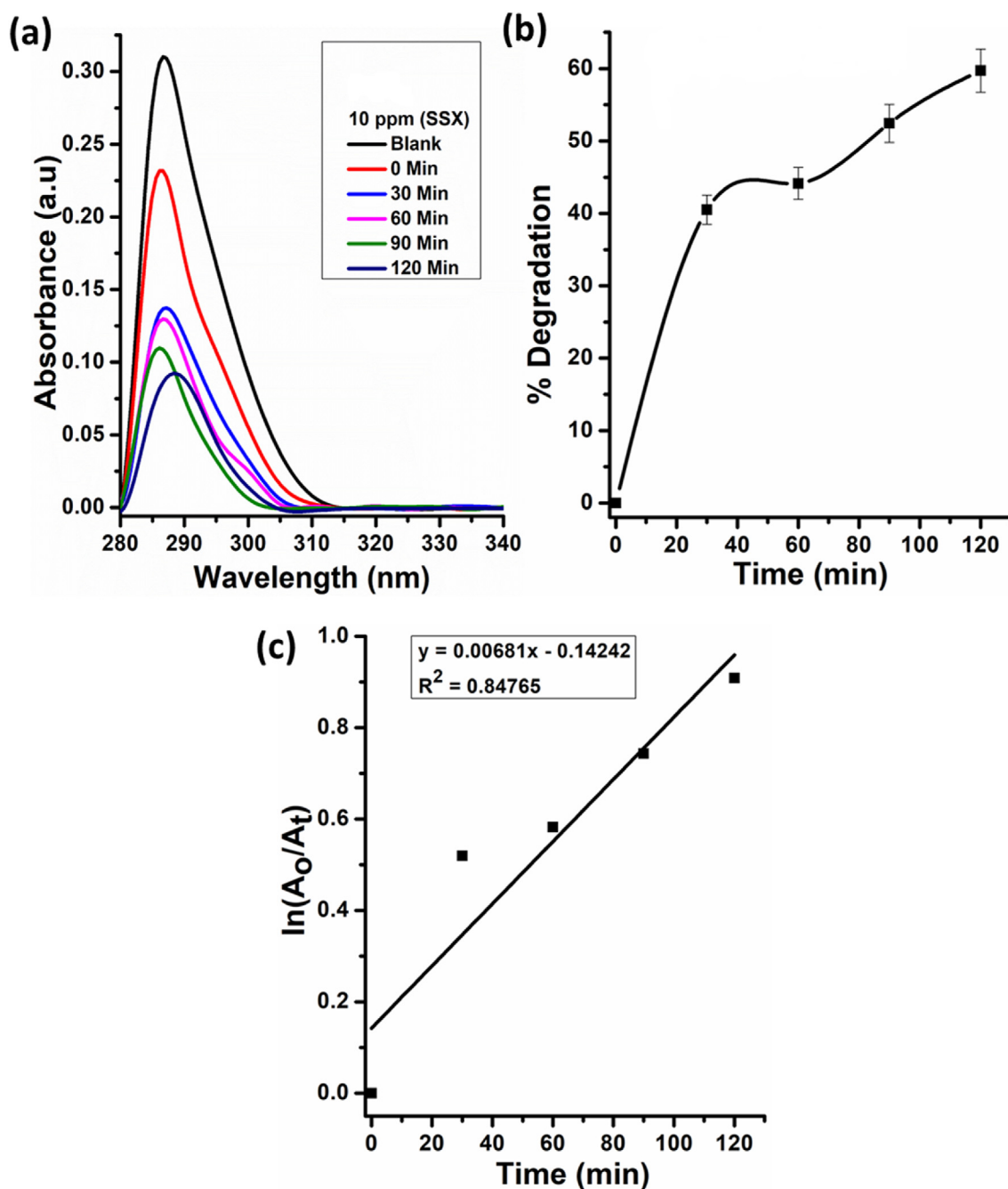
Figure 10. (a) Uv degradation spectra of Fe_3O_4 against the antibiotic SSX, (b) the degradation % of SSX versus the time and (c) kinetic plot versus time.

were all the strains detected. Upon treating these various water bodies using *M. burkeana* Fe_3O_4 NPs with 2 differing concentrations, for tap water which had the least number of microbes and only total coliforms, a 100% removal was noted at the highest concentration of the catalyst. In pond water, only a 98% removal could be achieved for total coliform and *S. aureus*. In both river and sewage water, a 100% total removal of *S. aureus* was achieved even at the lowest concentration. In sewage water the total coliform even after treatment with the highest concentration, was still very high. From this analysis it can be concluded that our synthesized material was more potent towards gram positive strains. Generally it is expected that the highest potency will be achieved against gram negative strains since they have a single peptidoglycan layer, they should be more prone to the breakdown of the bacterial cell but surprisingly as noted in the sewage water, the *E. coli* was highly resistant.

Several factors other than the cell wall of the strains can play a role in the potency of the material, factors such as the formation of the radical species, particle size, morphology and stability also can be factored in. Also, other studies have noted that because of the positive charge of the metal cation and negative charge of the bacteria, due to the attraction, these materials become equally enticed, which then results in a denaturation of the proteins, resulting in the destruction of the pathogen. The efficiency of nanoparticles against gram positive strains more than gram negative strains though it is not expected it is also not unusual as several studies have reported such a pattern before [19]. Furthermore, it is known that gram negative strains tend to be defiant against several antibodies since their cell wall though thin can be impenetrable. This study has therefore shown that our green derived iron oxide material can be used for the degradation and removal of several pollutants in water.

Table 2. Effect of Fe₃O₄ NPs against various bacterial strains in real water samples.

Water sample		Total coliform	E coli	S aureus
Pond	A	1.7×10^3	0	66
	B	2.0×10^2	0	53
	C	10	0	10
River	A	5.8×10^3	0	1.0×10^2
	B	67	0	0
	C	10	0	0
Tap	A	1.0×10^2	0	0
	B	30	0	0
	C	0	0	0
Sewage	A	4.9×10^4	3.0×10^4	50
	B	2.0×10^3	67	0
	C	1.3×10^3	10	0

4. Conclusion

This study has successfully reported on the green synthesis Fe₃O₄ NPs as confirmed as by FTIR, XRD, EDS, SEM, BET, TGA and DTG. FTIR confirmed the presence of carbohydrate groups from the plant extract on the synthesized Fe₃O₄ NPs. The characteristic peaks of Fe₃O₄ NPs were observed on the XRD plots of the green synthesized NPs, with this information, the crystallites sizes were calculated and found to be around 60 nm for the green synthesized NPs. DTA and TGA revealed the presence of organic moieties on the synthesized NPs, with their decomposition identified between 450–600 °C. BET analysis showed that Fe₃O₄ NPs was mesoporous in structure, meaning that their structure can adsorb and degrade organic and antibiotic pollutants. Fe₃O₄ was effective in degrading the organic and the antibiotic pollutants, obtaining the highest degradation of 99 and 60% removal for MB and SSX, respectively. The kinetic followed first order and seconder kinetics for the MB and SSX, respectively. The superoxide was the most effective radical followed by the electrons radical on the trapping studies. The reusability study for our material revealed that Fe₃O₄ was stable and recyclable for over 4 cycles. Lastly, upon testing the antibacterial efficiency of our material using real water from various sources, the Fe₃O₄ NPs were more potent against gram positive strains than negative.

Declarations

Author contribution statement

LM Mahlaule-Glory: Performed the experiments; Analyzed and interpreted the data; Wrote the paper. S Mapetla, A Makofane, M Mathipa: Performed the experiments; Analyzed and interpreted the data. NC Hintsho-Mbita: Conceived and designed the experiments; Analyzed and interpreted the data; Contributed reagents, materials, analysis tools or data; Wrote the paper.

Data availability statement

Data will be made available on request.

Declaration of interest statement

The authors declare no conflict of interest.

Additional information

No additional information is available for this paper.

References

[1] M.J.K. Ahmed, M. Ahmaruzzaman, M.H. Bordoloi, Novel averrhoa carambola extract stabilized magnetite nanoparticles: a green synthesis route for the removal of chlorazol black e from wastewater, RSC Adv. 5 (91) (2015) 74645–74655.

[2] M.F. Al-Hakkani, G.A. Gouda, S.H.A. Hassan, A review of green methods for phyto-fabrication of hematite (α-Fe2O3) nanoparticles and their characterization, properties, and applications, Heliyon 7 (2021), e05806.

[3] P.O. Akinola, A. Lateef, T.B. Asafa, L.S. Beukes, A.S. Hakeem, H.H. Irshad, Multifunctional titanium dioxide nanoparticles biofabricated via phytosynthetic route using extracts of Cola nitida: antimicrobial, dye degradation, antioxidant and anticoagulant activities, Heliyon 6 (2020) pe04610.

[4] S. Anchan, S. Pai, H. Sridevi, T. Varadavenkatesan, R. Vinayagam, R. Selvaraj, Biogenic synthesis of ferric oxide nanoparticles using the leaf extract of Peltophorum pterocarpum and their catalytic dye degradation potential, Biocatal. Agric. Biotechnol. 20 (2019), 101251.

[5] L. Ardakani, V. Alimardani, A.M. Tamaddon, A.M. Amani, S. Taghizadeh, Green synthesis of iron-based nanoparticles using Chlorophytum comosum leaf extract: methyl orange dye degradation and antimicrobial properties, Heliyon 7 (2021), e06159.

[6] A. Bahadur, A. Saeed, M. Shoaib, S. Iqbal, M.I. Bashir, M. Waqas, Eco-friendly synthesis of magnetite (Fe₃O₄) nanoparticles with tunable size: dielectric, magnetic, thermal and optical studies, Mater. Chem. Phys. 198 (2017) 229–235.

[7] M.S.H. Bhuiyan, M.Y. Miah, S.C. Paul, T. Aka. Das, O. Saha, M.M. Rahaman, M.J.I. Sharif, O. Habiba, M. Ashaduzzaman, Green synthesis of iron oxide nanoparticle using Carica papaya leaf extract: application for photocatalytic degradation of remazol yellow RR dye and antibacterial activity, Heliyon 6 (2020).

[8] I. Bibi, N. Nazar, S. Ata, M. Sultan, A. Ali, A. Abbas, K. Jilani, S. Kamal, F.M. Sarim, M.I. Khan, F. Jalal, M. Iqbal, Green synthesis of iron oxide nanoparticles using pomegranate seeds extract and photocatalytic activity evaluation for the degradation of textile dye, J. Mater. Res. Technol. 8 (2019) 6115–6124.

[9] H.S. Devi, M.A. Boda, M.A. Shah, S. Parveen, A.H. Wani, Green synthesis of iron oxide nanoparticles using *Platanus orientalis* leaf extract for antifungal activity, Green Process. Synth. 8 (2019) 38–45.

[10] R.B. González-González, A. Sharma, R. Parra-Saldívar, R.A. Ramirez-Mendoza, M. Bilal, H.M.N. Iqbal, Decontamination of emerging pharmaceutical pollutants using carbon-dots as robust materials, J. Hazard Mater. 423 (2022) 127.

[11] A. Hojjati-Najafabadi, M. Mansoorianfar, T. Liang, K. Shahin, H. Karimi-M, A review on magnetic sensors for monitoring of hazardous pollutants in water resources, Sci. Total Environ. 824 (2022), 153844.

[12] I.E. Juárez-Rojop, C.A. Tovilla-Zárate, D.E. Aguilar-Domínguez, LFR Fuente de la, C.E. Lobato-García, J.L. Blé-Castillo, L. López-Meraz, J.C. Díaz-Zagoya, D.Y. Bermúdez-Oca, Phytochemical screening and hypoglycemic activity of carica papaya leaf in streptozotocin-induced diabetic rats, Brazilian J Pharmacogn 24 (2014) 341–347.

[13] H.F. Kiwumulo, H. Muwonge, C. Ibingra, M. Lubwana, J.B. Kiraba, R.T. Ssekitoleko, Green synthesis and characterization of iron-oxide nanoparticles using Moringa oleifera: a potential protocol for use in low and middle income countries, BMC Res. Notes 15 (2022) 149.

[14] A. Lateef, T.B. Asafa, L.S. Beukes, A.S. Hakeem, H.H. Irshad, Multifunctional titanium dioxide nanoparticles biofabricated via phytosynthetic route using extracts of Cola nitida: antimicrobial, dye degradation, antioxidant and anticoagulant activities, Inorg. Chem. Commun. 6 (2020), e04610.

[15] A. Makofane, P. Maake, M.M. Mathipa, N.M. Matinise, F. Cummings, D.E. Motaung, N.C. Hintsho-Mbita, Green synthesis of NiFe₂O₄ nanoparticles for the photocatalytic degradation of methylene blue, sulfisoxazole and bacterials strains, Inorg. Chem. Comm 139 (2022), 109348.

[16] S. Lakshmnarayanan, M.F. Shereen, K.L. Niraimathi, P. Brindha, A. Arumug, One-pot green synthesis of iron oxide nanoparticles from Bauhinia tomentosa: characterization and application towards synthesis of 1, 3 diolein, Sci. Rep. 11 (2021) 1–13.

[17] N. Latha, M. Gowri, Bio synthesis and characterization of Fe₃O₄ nanoparticles using *Caricaya* papaya leaves extract, Int. J. Sci. Res. 3 (2014) 1551–1556.

[18] K. Motene, L.M. Mahlaule-Glory, N.M. Ngoepe, M.M. Mathipa, N.C. Hintsho-Mbita, Photocatalytic degradation of dyes and removal of bacteria using biosynthesised flowerlike NiO nanoparticles, Int. J. Environ. Anal. Chem. (2022) 1–16.

[19] N.M. Ngoepe, M. M Mathipa, N.C. Hintsho-Mbita, Biosynthesis of titanium dioxide nanoparticles for the photodegradation of dyes and removal of bacteria, Optik 224 (2020), 165728.

[20] M. Senhil, C. Ramesh, Biogenic synthesis of Fe₃O₄ nanoparticles using *Tridax procumbens* leaf extract and its antibacterial activity on *Pseudomonas aeruginosa*, J. Nanomat. Biostruc. 7 (2022) 1655–1660.

[21] S.J. Olusegun, G. Larrea, M. Osial, K. Jackowska, P. Krysinski, Photocatalytic degradation of superparamagnetic iron oxide nanoparticles.Tetracycline case, Catalyst 11 (2021) 1243.

[22] M. Pattanayak, P.L. Nayak, Ecofriendly green synthesis of iron nanoparticles from various plants and Spices extracts, Int. J. Plant Animal Env. Sci. 3 (2013) 68–78.

[23] T.M.H. Pham, M.T. Vu, T.D. Cong, N.S. Nguyen, T.A. Doan, T.T. Truong, T.H. Nguyen, Green sonochemical process for preparation of polyethylene glycol–Fe₃O₄/ZnO magnetic nanocomposite using rambutan peel extract as photocatalyst for removal of methylene blue in solution, Bull. Mater. Sci. 1 (2022) 1–10.

[24] S. Yogamoorthi, A. Kalidasan, Preparation and structural characterization of Iron Oxide nanoparticles from Iron rust-a novel material and eco-friendly method, J. Nano Vision. 3 (2013) 84–92.

[25] S.D. Roy, K.C. Das, S.S. Dhar, Conventional to green synthesis of magnetic iron oxide nanoparticles; its application as catalyst, photocatalyst and toxicity: a short review, Inorg. Chem. Commun. 134 (2021), 109050.

[26] S. Qasim, A. Zafar, M.S. Saif, Z. Ali, M. Nazar, M. Waqas, A.U. Haq, T. Tariq, S.G. Hassan, F. Iqbal, X.G. Shu, M. Hasan, Green synthesis of iron oxide nanorods using Withania coagulans extract improved photocatalytic degradation and antimicrobial activity, J. Photochem. Photobiol. B Biol. 204 (2020), 111784.

[27] S. Vasantharaj, S. Sathiyavimal, P. Senthilkumara, F.L. Oscar, A. Pugazhendhid, Biosynthesis of iron oxide nanoparticles using leaf extract of Ruellia tuberosa: antimicrobial properties and their applications in photocatalytic degradation, J. Photochem. Photobiol. B Biol. 192 (2019) 74–82.

[28] A.R. Singh, P.S. Dhumal, M.A. Bhakare, K.D. Lokhande, M.P. Bondarde, In-situsynthesis of metal oxide and polymer decorated activated carbon-basedphotocatalyst for organic pollutants degradation, Separ. Purif. Technol. 286 (2022), 120380.

[29] K. Saravanakumar, S. SivaSantosh, A. Sathiyaseelan, K.V. Naveen, M.A. AfaanAhamed, X. Zhang, V.V. Priya, D. MubarakAli, M.-H. Wang, Unraveling the hazardous impact of diverse contaminants in the marine environment: detection and remedial approach through nanomaterials and nano-biosensors, J. Hazard Mater. (2022), 128720.

[30] A. Saravanan, P. Senthil Kumar, S. Jeevanantham, S. Karishma, B. Tajsabreen, P.R. Yaashikaa, B. Reshma, Effective water/wastewater treatment methodologies for toxic pollutants removal: processes and applications towards sustainable development, Chemosphere 280 (2021), 130595.

[31] C. Sudhakar, M. Poonkothai, T. Selvankmuar, K. Selvam, G. Rajivgandhi, M.Z. Siddiqi, N.S. Alharbi, S. Kadaikunnan, N. Vijayakumar, et al., Biomimetic synthesis of iron oxide nanoparticles using Canthium coromandelicum leaf extract and its antibacterial and catalytic degradation of Janus green, Inorg. Chem. Commun. 133 (2021), 108977.